Organic Electronics 75 (2019) 105389

Contents lists available at ScienceDirect

Organic Electronics

journal homepage: www.elsevier.com/locate/orgel

Random lasing in brain tissues

F. Lahoz[a,*], A. Acebes[b], T. González-Hernández[b], S. de Armas-Rillo[a], K. Soler-Carracedo[a], G. Cuesto[b], V. Mesa-Infante[b]

[a] Departamento de Física, IUdEA, Universidad de La Laguna, Santa Cruz de Tenerife, Spain
[b] Departamento de Ciencias Médicas Básicas, Instituto de Tecnologías Biomédicas (ITB), Universidad de La Laguna, Santa Cruz de Tenerife, Spain

ARTICLE INFO

Keywords:
Random lasing
Light tissue interactions
Dye lasers
Biophotonics
Biological sensors

ABSTRACT

Brain is arguably the most complex organ in biology. It shows a heterogeneous structure, in which different areas are responsible for different functions. New non-invasive techniques to monitor the structure and/or composition of the brain can help to understand this organ. In this paper, we show successful random lasing from a mouse brain tissue impregnated with a dye laser and demonstrate that it can be used to detect changes in structure and composition. We systematically observe that the lowest random lasing threshold and highest intensity are recorded in the corpus callosum anatomical region of the brain. This area is formed by a large number of axon fibers coated by myelin, which is a lipid rich substance. Both the fiber structure and the lipid rich composition contribute to increase the scattering strength, which improves random lasing. A thorough photoluminescence characterization of the tissues as a function of the staining concentrations is also included in the study.

1. Introduction

Random lasing (RL) is obtained in media, which provide both light amplification through stimulated emission and optical feedback through multiple scattering processes. This phenomenon was first proposed more than 50 years ago [1,2], but it has been especially developed in the last two decades for its ground physics and applications [3–7]. RL can be easily achieved by combining efficient laser dye molecules with a scattering environment [8–11]. RL is particularly appealing in biological environments, which offer scattering surroundings. In this sense, RL was successfully reported in dye impregnated human tissues. Moreover, changes in the RL characteristics allowed differentiating cancerous from healthy surrounding tissues [12,13]. In addition to this, RL was also reported in individual cells [14], bone tissues [15,16], insect wings [17,18], bovine heart [19] or in fat, muscle, nerve and skin pig tissues [20]. Conventional laser dyes were used in most of these studies. Nevertheless, RL was also demonstrated in biological tissues impregnated with a fluorescent drug, formed by the covalent binding of a small dye molecule to a drug moiety, which is used in breast cancer therapy [21].

Despite the large amount of RL investigations for biological applications, as far as we are aware, no research on RL in brain tissues has ever been conducted. Currently, there is a great interest in understanding brain anatomy and function in animal models and human beings by employing multidisciplinary approaches. Moreover, large international consortiums have been developed to achieve this goal [22–24]. Therefore, the demonstration of RL in brain tissues would be of great interest because it would introduce RL as a new optical tool for the study of this complex organ.

In this paper, we present successful results on RL in mouse brain tissues impregnated with Rhodamine 6G (R6G). Four different R6G concentrations were tested and their effects on the RL properties of the stained brain tissues were analyzed. Unlike other tissues, brain is a rather heterogeneous one, in which different regions (cerebral cortex, corpus callosum, striatum, etc) might show different dye impregnation rates and/or scattering strengths. For this reason, we have performed RL experiments in different regions of the brain and mappings of the fluorescence signal of the stained brain slices were evaluated. Based on our data the heterogeneity in RL properties throughout the brain tissues was discussed.

2. Experimental

2.1. Brain tissue preparation

The experiments were carried out on C57BL/6 male mice (n = 6). Experimental protocols were approved by the Ethical committee of the University of La Laguna (Reference # CEIBA2013-0083), and are in

* Corresponding author.
E-mail address: flahoz@ull.es (F. Lahoz).

https://doi.org/10.1016/j.orgel.2019.105389
Received 7 June 2019; Received in revised form 25 July 2019; Accepted 31 July 2019
Available online 01 August 2019

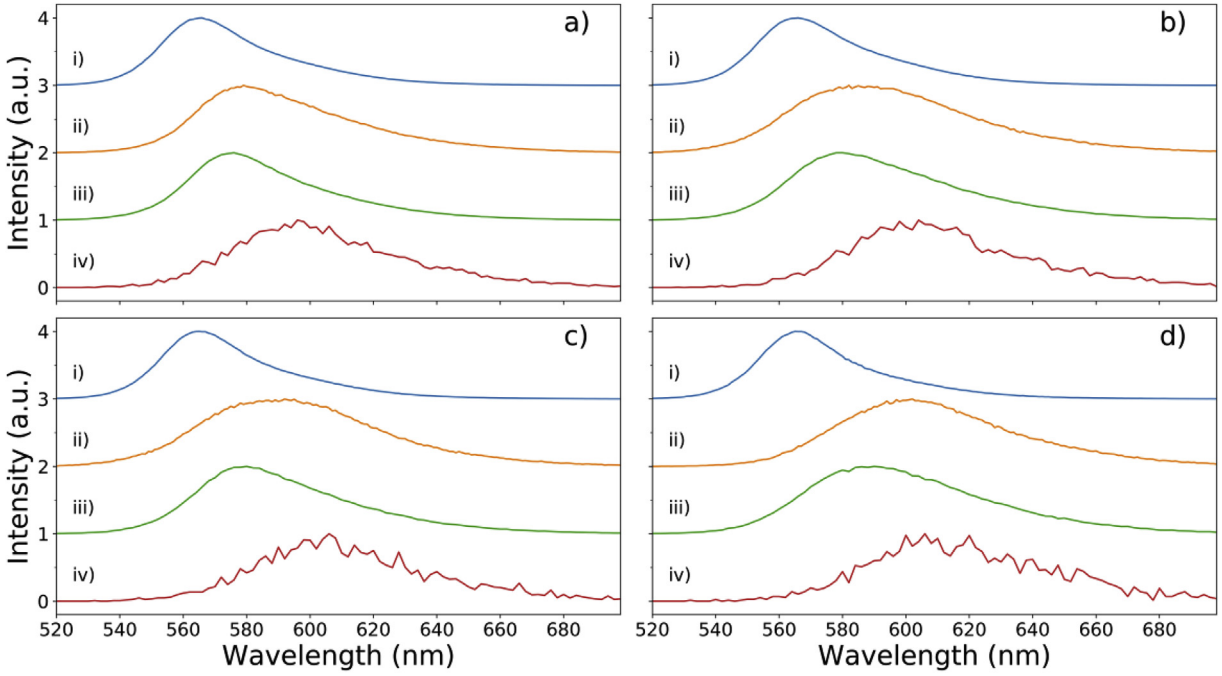

Fig. 1. Emission spectra of i) R6G/EtOH solutions, impregnated brain tissues measured in ii) quasi steady-state regime, iii) time-resolved at t = 0 ns, iv) time-resolved at t = 9 ns. Panels correspond to a) 5 mM, b)10 mM, c) 20 mM and d) 50 mM R6G/EtOH concentrations.

accordance with the European Communities Council Directive of 22 September 2010 (2010/63/EU). Mice were deeply anesthetized with an overdose of sodium pentobarbital and transcardially perfused with heparinized ice-cold 0.9% saline (30 ml) followed by 4% paraformaldehyde in phosphate buffered saline pH 7.4 (PBS, 50 ml). Brains were removed and stored overnight in the same fixative at 4 °C. Four of them were cryoprotected in sucrose 30% in PBS and stored at −80 °C until processing. Coronal sections (100 µm) were obtained with a freezing microtome and collected in 6 parallel series. The other two brains were dehydrated, and embedded in paraffin under standard conditions. Serial coronal sections of 10 µm were stained with the Kluver-Barrera method.

2.2. Brain tissue staining process

The brain staining process was performed at room temperature. The sucrose 30% in PBS medium used for brain cryoprotection was removed and substituted by an ethanol solution (1 ml) containing R6G (concentrations used 5, 10, 20 and 50 mM). Brain slices remained in the R6G/EtOH medium for 1 h. Then, they were rinsed in PBS four times before use.

2.3. Fluorescence characterization

Fluorescence measurements were performed using an Edinburgh Instruments LifeSpec II fluorescence spectrometer, exciting the complexes at 470 nm with an Edinburgh Instruments EPL-470 ps pulsed diode laser working in the MHz repetition range (temporal pulse width at half maximum about 80 ps) and using Edinburg Instruments F900 acquisition software. A multichannel plate photomultiplier was used as the detector using single photon counting technique. Lifetime estimation was made using instrument response function (IRF) reconvolution analysis with FAST software by Edinburgh Instruments, providing a temporal resolution around 0.03 ns.

The mappings of the integrated emission intensity of the stained brain slices were performed with a confocal microscope (Renishaw, inVia) equipped with a 532 nm laser line and a motorized translation stage for the sample holder, allowing controlled change of the position of the sample. A 20× microscope objective, with a long working distance (25 mm), was used to perform the fluorescence based imaging of the brain. The same microscope objective was used to excite the sample and to collect the fluorescence from the pumped area. The excitation spot had a diameter of about 2 µm. In order to obtain the image, measurements were taken every 100 µm both in the X and Y directions of the brain plane.

2.4. Random lasing characterization

A frequency doubled Nd-YAG pulsed laser oscillating at 532 nm was used as the excitation source. It provides laser pulses of about 8 ns at a repetition rate of 10 Hz. A pinhole was placed in front of the pump laser to select a homogenous excitation beam. Two linear polarizers were used to modulate the intensity of the pump beam. A cylindrical lens focused the pump beam on the sample with normal incidence to form a horizontal line 2.5 mm long and 0.5 mm wide. The emission of the sample was collected at an angle of about 30° from the normal direction with a convergence lens. A fiber coupled CCD spectrometer was used to analyze the emitted light. The best spectral resolution available was 0.05 nm. The thickness of the brain tissues used in the RL experiments was 200 µm.

3. Results and discussion

3.1. Fluorescence properties

Brain slices were soaked in R6G/EtOH solutions at four different concentrations (5, 10, 20 and 50 mM). The fluorescent properties of the tissues were analyzed as a function of the soaking concentration. First, the quasi steady-state emission spectra of the tissues were measured using a picosecond pulsed laser at 470 nm working at 20 MHz and integrating the emission of the sample over time. Then, time-resolved emission spectroscopy was performed to obtain the emission spectra just after the pump pulses (t = 0 ns) and 10 ns after the pump pulses (t = 10 ns). Additionally, the quasi steady-state emission of the dye solution used for the impregnation was also performed. All these data are given in Fig. 1 for the four different dye concentrations used in this

Table 1
Fluorescence parameters of R6G/EtOH impregnated mouse brain tissues as a function of the soaking concentration. The spectroscopic parameters of the soaking solutions are also given for comparison.

R6G/EtOH concentration (mM)	λ_{em} (± 0.5 nm)	FHHM (± 1 nm)	τ (± 0.1 ns)	τ_{av} at 580 nm (± 0.2 ns)	τ_{av} at 620 nm (± 0.2 ns)
5 (tissue)	579	50		0.8	2.9
10 (tissue)	582	63		1.6	2.8
20 (tissue)	592	63		1.3	2.3
50 (tissue)	602	60		1.1	2.3
5 (solution)	566	37	5.0		
10 (solution)	566	38	3.3		
20 (solution)	565	36	1.2		
50 (solution)	565	34	0.4		

study. The fluorescence properties of the impregnated tissues are summarized in Table 1. The spectroscopic parameters of the soaking solutions are also included for comparison.

The emission spectra of the R6G/EtOH solutions showed a maximum at about 565 nm and a similar full width at half maximum (FWHM) in the range of about 34–38 nm for all the concentrations. The intensity of the emission strongly decreased as the dye content in the solution increased. It is well known that R6G molecules tend to aggregate to form dimers and other aggregates when the dye concentration is high [25–28]. Our results suggested that the emissions of R6G/EtOH solutions were mainly due to monomers and they were partly quenched by energy transfer from excited state monomers to ground state non-fluorescent dimers when the dye concentration increased. Similar behaviors were previously reported [28–30]. When the brain slices were immersed in the dye solutions, these molecules penetrated the tissues. The emission spectra of the stained brain tissues were red-shifted and broader than those of the liquid solutions. R6G dye molecules in solid samples could exist as monomers, dimers and high-order aggregated forms, especially for high dye loading concentrations. Dimers can be luminescent, the so called J-type dimers, or non-luminescent, H-type dimers, depending on their geometrical arrangement, and high-order aggregates show a poor fluorescent character [31,32]. Both the observed red-shift of the emission spectra and the broadening of the bands seemed to indicate that the emissions of the impregnated tissues were due to luminescent aggregates and that the emission of monomers was strongly quenched by energy transfer to aggregates. Indeed, the emission spectra of the tissues were mainly due to luminescent J-type dimers, and to higher-order aggregates, especially for the 50 mM stained tissue, which emitted at longer wavelengths [31–33].

Time-resolved emission spectra showed a red-shift of the emission from 0 to 10 ns after the pump pulses, which was more evident as the R6G/EtOH concentration increased, in agreement with other reports on dye doped solid films [32]. At time 0 ns, that is, just after the pump pulse, both dimers and high-order aggregates contribute to the emission spectra. However, 10 ns after the pump pulse the emission spectra could be mainly attributed to high-order aggregates, which were red-shifted as compared to dimers. The highest red-shift was observed for the 50 mM impregnated tissue, for which high-order aggregates were expected [32].

The decays of the fluorescence of the impregnated brain tissues detecting at 580 and 620 nm are given in Fig. 2 as a function of the staining concentration used. The decays of the dye solutions detecting at 565 nm are also included in the figure for comparison. The intensity decays of the fluorescence of the dye solutions showed an exponential behavior and could be fitted to the expression:

$$I(t) = Ae^{\left(-\frac{t}{\tau}\right)} \quad (1)$$

Where A represents the intensity at t = 0 ns, and τ means the decay constant of the excited level. The value of τ was 5.0 ns for the 5 mM R6G/EtOH solution and decreased to 3.3, 1.2, and 0.4 as the concentration increased to 10, 20 and 50 mM, respectively. The reduction of τ as the dye concentration increases was due to energy transfer from the excited state of monomers to the ground state of non-radiative aggregates. The drop of τ in the solutions was accompanied by a quenching of the emission intensity, in agreement with other reports [28–30,34].

The fluorescent behavior of R6G in the brain tissues was much more complicated than in the solutions, as it normally happens in solid films, because several types of fluorescent aggregates, energy transfer processes between aggregates, and interaction of the R6G molecules with a non-homogeneous environment may occur [31,32]. All these phenomena led to a non-exponential decay as it can be observed in Fig. 2. In this case, the decay curves were fitted to a multi-exponential decay of the form

$$I(t) = A_1 e^{\left(-\frac{t}{\tau_1}\right)} + A_2 e^{\left(-\frac{t}{\tau_2}\right)} + A_3 e^{\left(-\frac{t}{\tau_3}\right)} \quad (2)$$

Where A_i and τ_i represent the pre-exponential factor and decay constant of the i-th component of the decay curve. Equation (2) is useful to define an average decay constant, τ_{av}, as

$$\tau_{av} = \frac{A_1\tau_1^2 + A_2\tau_2^2 + A_3\tau_3^2}{A_1\tau_1 + A_2\tau_2 + A_3\tau_3} \quad (3)$$

Which represents an average time in which the molecules are in the excited state [35]. Fig. 2 shows a slower relaxation rate at longer wavelengths, 620 nm, than at shorter ones, 580 nm. Indeed, the average decay constant measured at 580 nm was in the range of 0.8–1.6 ns, for the different staining concentrations, while it increased to 2.3–2.8 ns when the fluorescence was recorded at 620 nm, as shown in Table 1. This result points to a longer average decay for the poorly luminescent high-order aggregates as compared to dimers, in agreement with the literature [32].

Random laser depends both on the gain properties and on the scattering strength of the media [36,37]. Therefore, the dye content of the tissue will play an important role on the RL characteristics. In order to determine the homogeneity of the dye distribution in the tissue, a mapping of the integrated emission intensity of the brain slice was performed. The averaged image of the brain obtained over 4 brain mappings is given in Fig. 3. There is not a clear preference of the dye to load a particular region of the brain. Indeed, the different areas of the brain (cortex, corpus callosum, striatum, amigdalar cortex) seem to be rather homogeneously impregnated. Some residual hotspots can be observed, which can be attributed to experimental artifacts due to the staining solution. We concluded that the R6G dye distribution shows no preference to accumulate in any particular anatomical brain region.

3.2. Random laser properties

The evolution of the fluorescence spectra with the pump energy is given in Fig. 4a for the brain slice impregnated with 5 mM R6G/EtOH. The characteristic broad band of R6G was observed at relatively low pump excitation. However, at a given pump energy, some narrow lines appeared superposed to the broad fluorescent band. These lines are associated to different lasing modes, which are excited in the brain. Moreover, the wavelength at which they are observed may change as the pump energy does, which has been reported for RL [5,6,9,14,17,21]. Indeed, the spectral width of the emission spectra narrows as the pump energy increases due to the appearance of RL peaks. Fig. 4b shows the evolution of the full width at half maximum (FWHM) and the emission intensity at the wavelength of the narrow lines as a function of the pump energy. Both the narrowing of FWHM due to the appearance of narrow lines and the sudden increase of the emission intensity are characteristics features of coherent RL and the pump energy at which it starts is the RL pump threshold. A RL threshold of about 45 μJ was found for the 5 mM R6G/EtOH impregnated tissue.

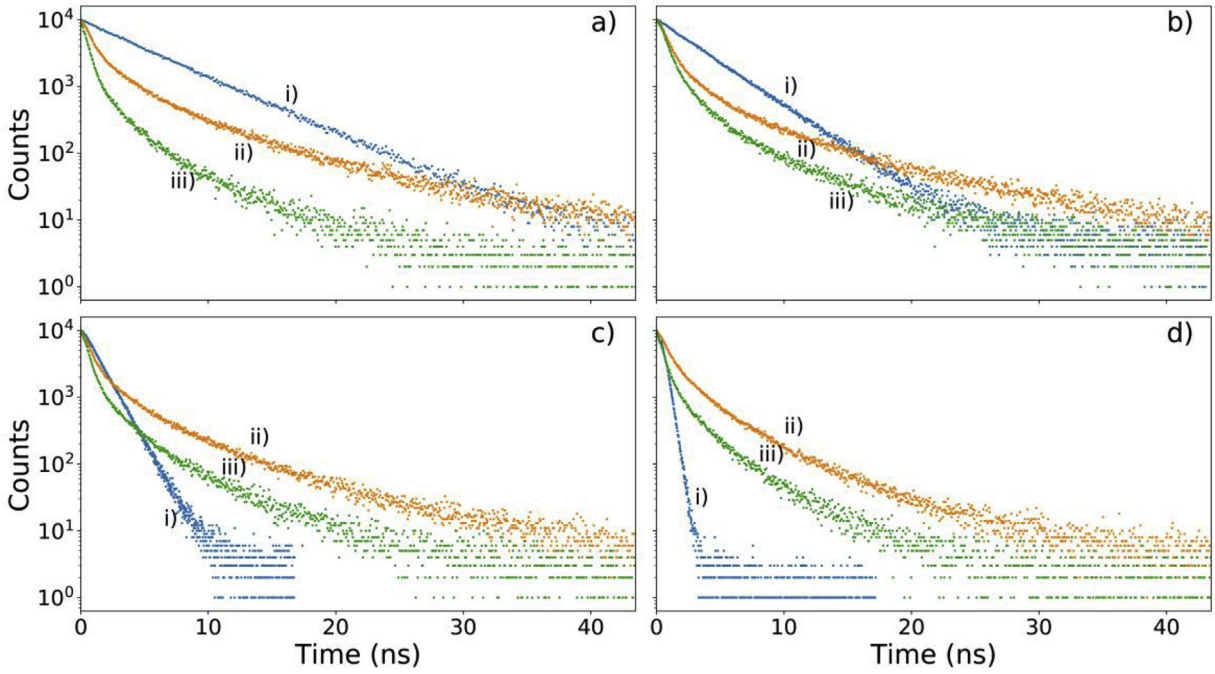

Fig. 2. Decay of the fluorescence of the starting solutions detected at i) 560 nm; and impregnated brain tissues measured at ii) 620 and iii) 580 nm. Panels correspond to a) 5 mM, b)10 mM, c) 20 mM and d) 50 mM R6G/EtOH concentrations.

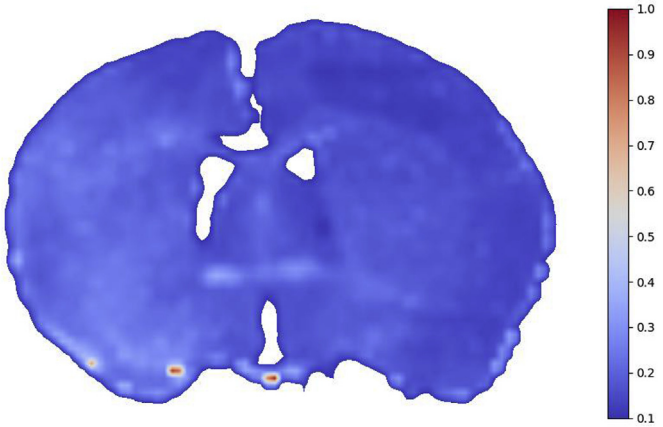

Fig. 3. Averaged mapping of the normalized integrated emission intensity of brain tissue impregnated with 5 mM R6G/EtOH.

Surprisingly, it slightly decreased to about 35 μJ at 10 mM R6G/EtOH concentration, see Fig. 4c. This reduction is opposed to the fluorescence quenching observed when the dye concentration was increased. However, RL is based on stimulated emission, which is different from the spontaneous emission of fluorescence and other factors must be taken into account. Indeed, the increase in the average decay constant measured at 580 nm means that R6G dimers stay longer in the excited state and remain available for stimulated emission photons, which would favor RL. When the used dye concentration further increased to 20 mM, RL threshold raised to some extent, 55 μJ. It considerably increased to about 120 μJ for the 50 mM R6G/EtOH soaked slice. This result is in agreement with the strong quenching of the fluorescence observed at high R6G concentrations because of the formation of poorly fluorescent high-order aggregates as mentioned before [31,32].

The fluorescence intensity was analyzed at low pump pulsed excitation, below RL threshold. The comparison of the fluorescence intensity in different anatomical regions of the brain confirmed that the dye distribution was independent of the brain region, as stated before.

In the RL experiments we observed photobleaching of the R6G dye molecules when the pump pulses exceeded an energy density around 320 μJ/mm^2. Taking into account the RL excitation area, it corresponds to a pulse energy of around 400 μJ. Therefore, RL spectra were obtained with single pulse excitation and we limited our practical range of pump energy to 200 μJ to avoid photobleaching. Under those pumping conditions, no apparent damage of the brain tissue was detected under microscope observation.

As previously mentioned, RL is obtained by the interaction of a gain medium with optical scatters. In our study, optical gain is provided by R6G molecules and the inner structure of the brain tissue is responsible for the scatters. The brain is composed of grey and white matter. The grey matter mostly contains glial cells and neurons (soma size in the range of 5–20 μm) limited by a lipid bilayer membrane, in which there exist a complex nano and microstructure due to a variety of organelles such as mitochondria, endoplasmic reticulum and nucleus among others. The white matter is formed by tracts of nerve fibers covered by myelin, a lipid sheath. All these elements represent inhomogeneities in terms of the optical path due to changes in the refractive index and may act as scatters in the RL phenomena. Additionally, the degree of disorder of the cells within the tissue and the intercellular medium may also contribute to the scattering in RL.

Due to the heterogeneity of the brain tissue, we mapped the RL threshold in different regions of the brain using the slice impregnated with 5 mM R6G, see Fig. 5a. The RL threshold depended on the excited area of the brain slice. The lowest threshold was detected in the corpus callosum region, 45 μJ, while higher values in the range of about 70–80 μJ were observed for the cortex, corpus striatum and amigdalar cortex. The same tendency was found when the brain tissues were stained at higher R6G concentrations.

RL spectra at different positions are shown in Fig. 6a for the 5 mM R6G/EtOH impregnation, at 158 μJ excitation energy per pulse, well above the RL threshold. The RL emission intensity was higher in the corpus callosum region. Indeed, the average RL intensity over four shots is given in Fig. 6b in four characteristic brain regions. Moreover, the highest RL intensity was systematically observed in the corpus callosum area regardless of the staining concentration.

Corpus callosum is a wide and thick fiber bundle formed by a large number of axons lying under the cerebral cortex that connects right and

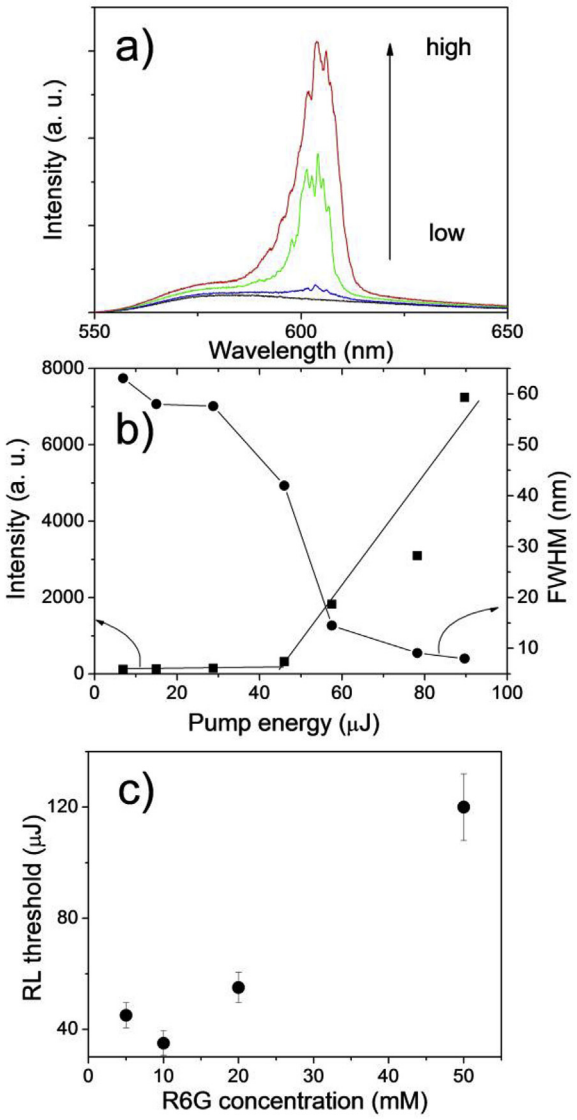

Fig. 4. a) Random lasing spectra, b) lasing intensity and FWHM as a function of pump energy of the brain tissue impregnated with 5 mM R6G; c) RL threshold versus R6G impregnating concentration. The excited area was around the corpus callosum.

left brain hemispheres. These fibers are coated by myelin, which is a lipid rich substance. The fiber-like structure of the corpus callosum area provides a non-isotropic environment, which favors scattering of light, see Fig. 5b and c. Additionally, the lipid rich composition of this region is associated with a higher refractive index [38]. This represents higher n contrast with aqueous interstitial spaces, providing higher light scattering efficiency. Both the fiber geometrical structure and the high n contrast are physiological factors which benefit scattering of light in the corpus callosum area. These factors explain both the lower RL threshold and higher RL intensity found in this region of the brain. Our findings are in agreement with the RL sensitivity to structure and composition of artificial tissue scaffolds recently reported [39].

Finally, it should be remarked that the narrow peaks (FWHM $<$ 1 nm) observed above the RL threshold correspond to defined coherent RL modes produced by scatters in the tissue. Since the brain tissue is a naturally non-homegeneous medium, the scattering centers are not uniformly distributed through the brain. Consequently, there may be brain regions in which the density of scatters is lower and lead to incoherent RL, characterized by narrow band (FWHM around 10–15 nm). In most cases, both contributions are observed. Moreover,

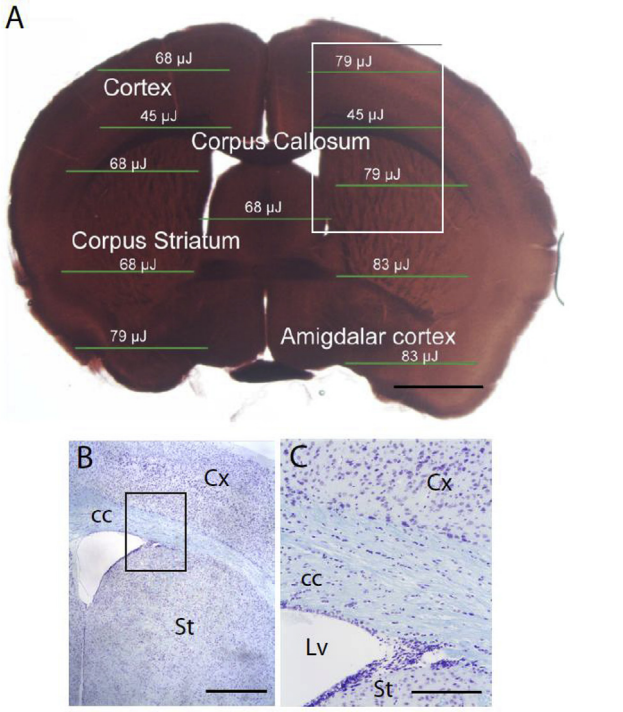

Fig. 5. A, coronal section of mouse brain stained with R6G showing the regions tested. Excitation areas are marked together with RL thresholds. B, Kluver-Barrera staining of a brain region corresponding to the area indicated in A. Neurons are stained purple and myelinated axons (corpus callosum) are stained blue. C, high magnification microphotograph of area indicated in B, myelinated axons run parallel to section plane. cc, corpus callosum; Cx, cerebral cortex; Lv, lateral ventricle; St, corpus striatum. Bar in A, 1.5 mm; Bar in B, 500 μm; Bar in C, 150 μm. (For interpretation of the references to colour in this figure legend, the reader is referred to the Web version of this article.)

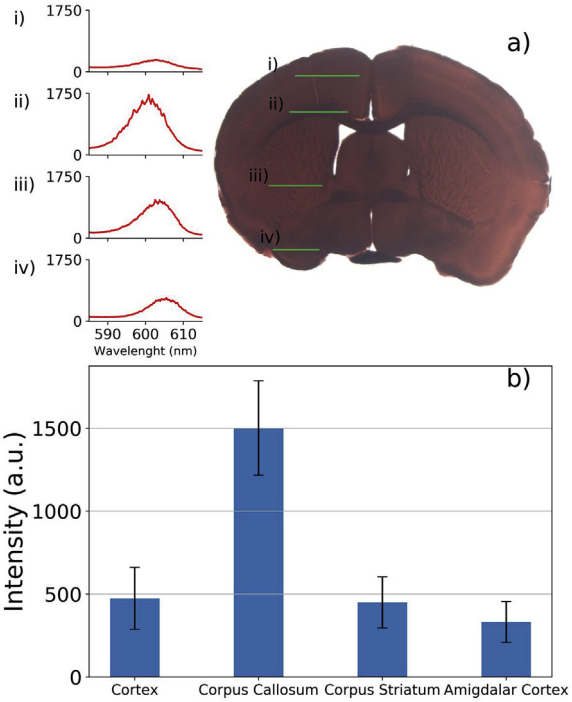

Fig. 6. a) RL spectra measured at different zones of the brain slice; b) average RL intensity measured at different zones (error bars represent standard deviation) for 5 mM and R6G/EtOH impregnated tissue.

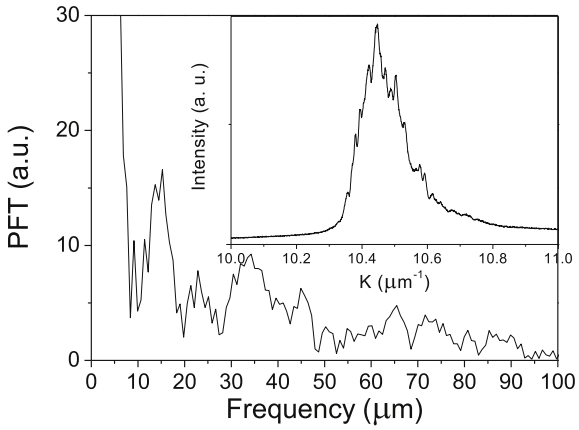

Fig. 7. PFT of coherent RL spectrum. Inset shows the RL spectrum as a function of wavenumber.

additional information about cavity size can be obtained by the Power Fourier Transformation (PFT) analysis of coherent RL spectrum. Briefly, the emission spectrum is represented as a function of the wave vector and PFT analysis is applied to obtain the Fourier component at frequency $p_m = m\ L_C\ n/\pi$, where m is the order of the Fourier harmonic, L_C is the cavity path length, and n is the refractive index of the medium [21]. As an example, Fig. 7 shows the PFT of a coherent RL spectrum. From the position of the PFT peaks, and assuming an average n of about 1.4, the lengths of the main coherent RL cavity modes range from 33 to 102 μm. This range of values indicated that some coherent RL cavity modes could exist within a single cell, while other modes could occur between cells and the intracellular medium.

4. Conclusions

The fluorescent and RL properties of brain tissues impregnated in highly concentrated R6G solutions (from 5 to 50 mM) were investigated. Time resolved fluorescence showed that the emission spectra were due to J-type dimers and high-order aggregates, which became dominant as the staining concentration increased.

RL was observed in all the stained brain slices. The RL threshold depended on the staining concentration. The lowest RL threshold, 35 μJ, was measured for the 10 mM stained tissue. Interestingly, RL threshold notably changed within the brain slice. For all the tissues used in this study the lowest RL threshold was detected when the excitation stripe was in the corpus callosum region. Moreover, when the brain tissues were scanned under a given pump power, the highest RL intensity was detected again in the corpus callosum area. RL depends both on the optical gain and on the scattering properties of the medium. Mapping of the spontaneous emission intensity of the brain tissues showed no significant enhancement of the emission in the corpus callosum region, discarding enriched dye impregnation of the corpus callosum as a reason of this behavior. Therefore, we concluded that the scattering strength of this brain region must be higher than in other areas of the brain. Indeed, both the lipid rich composition and the fiber like structure of this brain region improve the scattering strength favoring RL events. PFT analysis of the coherent RL spectra shows a range of RL cavity lengths which can occur inside single neuron cells and also between cells and intercellular medium. Finally, our results have demonstrated not only that RL can be achieved in stained brain tissues, but that RL can be used as an optical tool to detect composition/microstructural differences in the brain, which may have an influence on the scattering of light. The use of RL experiments in brain tissues shows the potential application to detect deficiencies in the lipid composition of the white matter as well as protein clusters in the grey matter, which can act as scattering centers enhancing RL characteristics. This would have a deep impact in neuroscience since demyelination and protein aggregation are main features in multiple sclerosis and neurodegenerative diseases, respectively. Further research is required to extend these investigations to other nervous tissues not restricted to the brain.

Acknowledgments

This research was supported by Ministerio de Economía, Industria y Competitividad, Spain (Agencia Estatal de Investigación, AEI) and European Union-FEDER (MAT2016-79866-R), (BFU2016-77363-R). Funding is also acknowledged to Gobierno Autónomo de Canarias, Agencia Canaria de Investigación, Innovación y Sociedad de la Información (ACIISI) (2018–00000034), (2018/00000022).

References

[1] R. Ambartsumyan, N. Basov, P. Kryukov, V. Letokhov, 5A10(b) - a laser with a nonresonant feedback, IEEE J. Quantum Electron. 2 (1966) 442–446, https://doi.org/10.1109/JQE.1966.1074123.
[2] V.S. Letokhov, Generation of light by a scattering medium with negative resonance absorption, Sov. J. Exp. Theor. Phys. 26 (1968) 835.
[3] D.S. Wiersma, A. Lagendijk, Light diffusion with gain and random lasers, Phys. Rev. E. 54 (1996) 4256–4265, https://doi.org/10.1103/PhysRevE.54.4256.
[4] H. Cao, Y.G. Zhao, H.C. Ong, S.T. Ho, J.Y. Dai, J.Y. Wu, R.P.H. Chang, Ultraviolet lasing in resonators formed by scattering in semiconductor polycrystalline films, Appl. Phys. Lett. 73 (1998) 3656–3658, https://doi.org/10.1063/1.122853.
[5] Y. Ling, H. Cao, A.L. Burin, M.A. Ratner, X. Liu, R.P.H. Chang, Investigation of random lasers with resonant feedback, Phys. Rev. A 64 (2001) 063808, , https://doi.org/10.1103/PhysRevA.64.063808.
[6] D.S. Wiersma, The physics and applications of random lasers, Nat. Phys. 4 (2008) 359–367, https://doi.org/10.1038/nphys971.
[7] B. Redding, M.A. Choma, H. Cao, Speckle-free laser imaging using random laser illumination, Nat. Photonics 6 (2012) 355–359, https://doi.org/10.1038/nphoton.2012.90.
[8] W.L. Sha, C.-H. Liu, R.R. Alfano, Spectral and temporal measurements of laser action of Rhodamine 640 dye in strongly scattering media, Opt. Lett. 19 (1994) 1922, https://doi.org/10.1364/OL.19.001922.
[9] R.C. Polson, Z.V. Vardeny, Organic random lasers in the weak-scattering regime, Phys. Rev. B. 71 (2005) 045205, , https://doi.org/10.1103/PhysRevB.71.045205.
[10] A. Costela, I. Garcia-Moreno, L. Cerdan, V. Martin, O. Garcia, R. Sastre, Dye-doped POSS solutions: random nanomaterials for laser emission, Adv. Mater. 21 (2009) 4163–4166, https://doi.org/10.1002/adma.200900799.
[11] L. Cerdán, A. Costela, E. Enciso, I. García-Moreno, Random lasing in self-assembled dye-doped latex nanoparticles: packing density effects, Adv. Funct. Mater. 23 (2013) 3916–3924, https://doi.org/10.1002/adfm.201202616.
[12] R.C. Polson, Z.V. Vardeny, Random lasing in human tissues, Appl. Phys. Lett. 85 (2004) 1289–1291, https://doi.org/10.1063/1.1782259.
[13] Y. Wang, Z. Duan, Z. Qiu, P. Zhang, J. Wu, D. Zhang, T. Xiang, Random lasing in human tissues embedded with organic dyes for cancer diagnosis, Sci. Rep. 7 (2017) 8385, https://doi.org/10.1038/s41598-017-08625-3.
[14] J. He, S. Hu, J. Ren, X. Cheng, Z. Hu, N. Wang, H. Zhang, R.H.W. Lam, H.-Y. Tam, Biofluidic random laser cytometer for biophysical phenotyping of cell suspensions, ACS Sens. (2019), https://doi.org/10.1021/acssensors.8b01188 acssensors.8b01188.
[15] Q. Song, S. Xiao, Z. Xu, J. Liu, X. Sun, V. Drachev, V.M. Shalaev, O. Akkus, Y.L. Kim, Random lasing in bone tissue, Opt. Lett. 35 (2010) 1425, https://doi.org/10.1364/OL.35.001425.
[16] Q. Song, Z. Xu, S.H. Choi, X. Sun, S. Xiao, O. Akkus, Y.L. Kim, Detection of nanoscale structural changes in bone using random lasers, Biomed. Opt. Express 1 (2010) 1401, https://doi.org/10.1364/BOE.1.001401.
[17] D. Zhang, G. Kostovski, C. Karnutsch, A. Mitchell, Random lasing from dye doped polymer within biological source scatters: the pomponia imperatorial cicada wing random nanostructures, Org. Electron. 13 (2012) 2342–2345, https://doi.org/10.1016/j.orgel.2012.06.029.
[18] H. Zhang, G. Feng, S. Wang, C. Yang, J. Yin, S. Zhou, Coherent random lasing from liquid waveguide gain channels with biological scatters, Appl. Phys. Lett. 105 (2014) 253702, https://doi.org/10.1063/1.4905035.
[19] J.C. Briones-Herrera, N. Cuando-Espitia, F.M. Sánchez-Arévalo, J. Hernández-Cordero, Evaluation of mechanical behavior of soft tissue by means of random laser emission, Rev. Sci. Instrum. 84 (2013) 104301, https://doi.org/10.1063/1.4823783.
[20] M. Hohmann, D. Dörner, F. Mehari, C. Chen, M. Späth, S. Müller, H. Albrecht, F. Klämpfl, M. Schmidt, Investigation of random lasing as a feedback mechanism for tissue differentiation during laser surgery, Biomed. Opt. Express 10 (2019) 807, https://doi.org/10.1364/BOE.10.000807.
[21] F. Lahoz, I.R. Martín, M. Urgellés, J. Marrero-Alonso, R. Marín, C.J. Saavedra, A. Boto, M. Díaz, Random laser in biological tissues impregnated with a fluorescent anticancer drug, Laser Phys. Lett. 12 (2015) 045805, , https://doi.org/10.1088/1612-2011/12/4/045805.
[22] H. Markram, The blue brain project, Nat. Rev. Neurosci. 7 (2006) 153–160, https://doi.org/10.1038/nrn1848.
[23] M.F. Glasser, S.M. Smith, D.S. Marcus, J.L.R. Andersson, E.J. Auerbach,

T.E.J. Behrens, T.S. Coalson, M.P. Harms, M. Jenkinson, S. Moeller, E.C. Robinson, S.N. Sotiropoulos, J. Xu, E. Yacoub, K. Ugurbil, D.C. Van Essen, The Human Connectome Project's neuroimaging approach, Nat. Neurosci. 19 (2016) 1175–1187, https://doi.org/10.1038/nn.4361.

[24] J.R. Ecker, D.H. Geschwind, A.R. Kriegstein, J. Ngai, P. Osten, D. Polioudakis, A. Regev, N. Sestan, I.R. Wickersham, H. Zeng, The BRAIN initiative cell census consortium: lessons learned toward generating a comprehensive brain cell atlas, Neuron 96 (2017) 542–557, https://doi.org/10.1016/j.neuron.2017.10.007.

[25] F. del Monte, J.D. Mackenzie, D. Levy, Rhodamine fluorescent dimers adsorbed on the porous surface of silica gels, Langmuir 16 (2000) 7377–7382, https://doi.org/10.1021/la000540+.

[26] G.M. Walker, L.R. Weatherley, Adsorption of dyes from aqueous solution — the effect of adsorbent pore size distribution and dye aggregation, Chem. Eng. J. 83 (2001) 201–206, https://doi.org/10.1016/S1385-8947(00)00257-6.

[27] M. Ogawa, N. Kosaka, P.L. Choyke, H. Kobayashi, H-type dimer formation of fluorophores: a mechanism for activatable, in vivo optical molecular imaging, ACS Chem. Biol. 4 (2009) 535–546, https://doi.org/10.1021/cb900089j.

[28] S. Terdale, A. Tantray, Spectroscopic study of the dimerization of rhodamine 6G in water and different organic solvents, J. Mol. Liq. 225 (2017) 662–671, https://doi.org/10.1016/j.molliq.2016.10.090.

[29] A. Penzkofer, W. Leupacher, Fluorescence behaviour of highly concentrated rhodamine 6G solutions, J. Lumin. 37 (1987) 61–72, https://doi.org/10.1016/0022-2313(87)90167-0.

[30] F.M. Zehentbauer, C. Moretto, R. Stephen, T. Thevar, J.R. Gilchrist, D. Pokrajac, K.L. Richard, J. Kiefer, Fluorescence spectroscopy of Rhodamine 6G: concentration and solvent effects, Spectrochim. Acta Part A Mol. Biomol. Spectrosc. 121 (2014) 147–151, https://doi.org/10.1016/j.saa.2013.10.062.

[31] V. Martínez Martínez, F. López Arbeloa, J. Bañuelos Prieto, T. Arbeloa López, I. López Arbeloa, Characterization of supported solid thin films of laponite clay. Intercalation of rhodamine 6G laser dye, Langmuir 20 (2004) 5709–5717, https://doi.org/10.1021/la049675w.

[32] V. Martínez Martínez, F. López Arbeloa, J. Bañuelos Prieto, I. López Arbeloa, Characterization of rhodamine 6G aggregates intercalated in solid thin films of laponite clay. 2 fluorescence spectroscopy, J. Phys. Chem. B 109 (2005) 7443–7450, https://doi.org/10.1021/jp050440i.

[33] C. On, E.K. Tanyi, E. Harrison, M.A. Noginov, Effect of molecular concentration on spectroscopic properties of poly(methyl methacrylate) thin films doped with rhodamine 6G dye, Opt. Mater. Express 7 (2017) 4286, https://doi.org/10.1364/OME.7.004286.

[34] F. López Arbeloa, P. Ruiz Ojeda, I. López Arbeloa, The fluorescence quenching mechanisms of Rhodamine 6G in concentrated ethanolic solution, J. Photochem. Photobiol. A Chem. 45 (1988) 313–323, https://doi.org/10.1016/S1010-6030(98)80004-X.

[35] J.R. Lakowicz (Ed.), Principles of Fluorescence Spectroscopy, Springer US, Boston, MA, 2006, , https://doi.org/10.1007/978-0-387-46312-4.

[36] X.H. Wu, A. Yamilov, H. Noh, H. Cao, E.W. Seelig, R.P.H. Chang, Random lasing in closely packed resonant scatterers, J. Opt. Soc. Am. B 21 (2004) 159, https://doi.org/10.1364/JOSAB.21.000159.

[37] X. Meng, K. Fujita, S. Murai, J. Konishi, M. Mano, K. Tanaka, Random lasing in ballistic and diffusive regimes for macroporous silica-based systems with tunable scattering strength, Opt. Express 18 (2010) 12153, https://doi.org/10.1364/OE.18.012153.

[38] J. Sun, S.J. Lee, L. Wu, M. Sarntinoranont, H. Xie, Refractive index measurement of acute rat brain tissue slices using optical coherence tomography, Opt. Express 20 (2012) 1084, https://doi.org/10.1364/OE.20.001084.

[39] S. Yang, S. Kim, H. Shin, S.H. Choi, Y.L. Kim, C. Joo, W. Ryu, Random lasing detection of structural transformation and compositions in silk fibroin scaffolds, Nano Res 12 (2019) 289–297, https://doi.org/10.1007/s12274-018-2213-7.